Short-term forecasting of the instantaneous wind velocity profile using a stochastic modeling approach

Marten Klein[1,2,*,ORCID: 0000-0003-0609-8961], Christoph Glawe[3,ORCID: 0000-0002-2172-7095], Mark Simon Schöps[1], Juan Alí Medina Méndez[1,ORCID: 0000-0002-1207-9604], and Heiko Schmidt[1,2,ORCID: 0000-0002-6475-6646]

[1] Lehrstuhl Numerische Strömungs- und Gasdynamik, Brandenburgische Technische Universität Cottbus-Senftenberg, Siemens-Halske-Ring 15A, 03046 Cottbus, Germany, WWW home page: https://www.b-tu.de/en/fg-stroemungsmodellierung
[2] Scientific Computing Lab, Energie-Innovationszentrum (EIZ), Brandenburgische Technische Universität Cottbus-Senftenberg, Platz der Deutschen Einheit 1, 03046 Cottbus, Germany, WWW home page: https://www.b-tu.de/en/energie-innovationszentrum
[3] wpd Onshore GmbH & Co. KG, Borsigstraße 8, 74321 Bietigheim-Bissingen, Germany, WWW home page: https://www.wpd.de/en
[*] Corresponding author.
E-mail addresses: marten.klein@b-tu.de (Marten Klein), heiko.schmidt@b-tu.de (Heiko Schmidt)

Abstract. A forward modeling strategy for short-term prediction of available wind energy is proposed based on the temporal evolution of atmospheric boundary layer profiles. The modeling approach utilizes the stochastic one-dimensional turbulence (ODT) model. ODT aims to provide extended, if not full-scale, vertical and temporal resolution. Atmospheric turbulence is modeled by a stochastic process, which is formulated with the aid of stochastically sampled mapping events that punctuate the otherwise continuous flow profile evolution. The model distinguishes advective from diffusive transport processes. In return, the model can capture laminar and turbulent response mechanisms. The turbulence intensity, occurrence, and range of scales is not prescribed, but a result of the momentarily available energy in the flow. It is demonstrated that the model can provide instantaneous velocity profiles and detailed velocity fluctuation statistics, bridging the gap from weakly to fully developed turbulent conditions.

Keywords: Atmospheric boundary layer; Intermittency; Stochastic modeling; Turbulent inflow
MSC codes: 76F25, 76F40, 82C31, 82C70

1 Introduction

Operational forecasting of available wind energy is continuing to gain importance with the incorporation of volatile renewable sources in the power grid.

Wind energy is one of the sources that reduce the inertia of the power grid. In order to improve grid stability, control is required. Control strategies can benefit from time-resolved forecasts of the instantaneous inflow velocity profile, that is, its evolution constrained by the local atmospheric conditions. There are various challenges associated with such forecasts. These challenges are foremost related to the capturing of the atmospheric inflow (e.g. [1, 2]), represented by evolving features in the velocity profile, like uniform momentum zones (e.g. [3, 4] and the coexistence of turbulent and laminar regions (e.g. [5, 6]), which represent only some of the additional complications which arise within wind farms (e.g. [7]). The day-ahead allocation of energy resources is, therefore, limited by the predictive capabilities and the resolution offered by the available numerical weather prediction (NWP) models. Taking ICON-D2 [8], the present operational NWP model of the German Weather Service (DWD), the spatial resolution is 2.2 km in the horizontal direction and 20 m in the vertical direction in the vicinity of the surface. Grid cells expand in height to 1.4 km toward the stratosphere so that 65 vertical mesh cell layers compose the relevant lower atmosphere, resolving a typical wind park with only a few grid cells. The time step is usually about 30–90 s. NWP-based approaches enable statistical day-ahead estimates of the available wind energy (e.g. [9]), but a detailed forecast on short time horizons as required for power grid control is not possible. Additional modeling (e.g. [4]) or a deconvolution strategy (e.g. [10–13]) may be adopted to obtain instantaneous velocity profiles for a selected site. Irrespective of the technical details of the approach taken, the desired numerical tool needs to be applicable to a variety of atmospheric flow conditions and able to capture the transient evolution of the atmospheric boundary layer (ABL).

Some of the standing challenges in modeling atmospheric boundary-layer turbulence may be addressed by considering the momentarily available energy in the flow. This is feasible to do when instantaneous flow profiles are evolved. Map-based advection modeling provides the necessary means to distinguish turbulent advection from diffusive transport processes. This approach is readily utilized in the so-called one-dimensional turbulence (ODT) model [14]. It has been demonstrated previously that ODT possesses relevant predictive capabilities for ABL flows. Application cases encompass stably stratified ABLs [15], surface roughness [16], and the response to transient forcings [5, 17]. The primary objective of the present paper, therefore, is to provide an overview of the regime-spanning forward modeling capabilities of ODT for applications in short-time wind energy forecasting. This covers weakly to fully developed turbulent wind fields that are traversed during morning and evening transitions. The present discussion remains limited to the neutrally stratified (shear-dominated) ABL, but the implemented model readily includes stratification effects [5, 15].

The rest of this paper is organized as follows. Section 2 provides an overview of the flow configuration and the applicable model formulation. Section 3 contains the key results and their discussion. Lastly, section 4 closes with some concluding remarks.

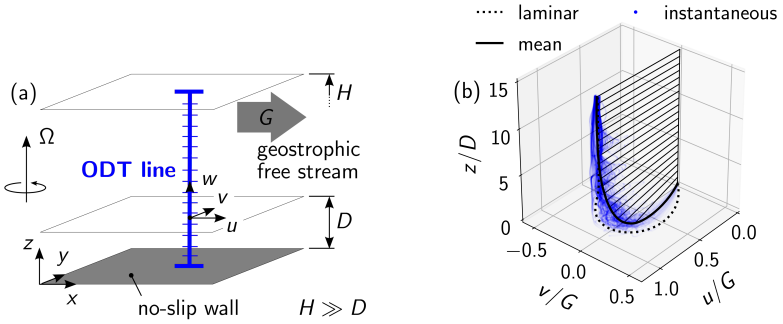

Fig. 1: (a) Sketch of the neutrally stratified ABL configuration investigated. The one-dimensional domain for the stochastic flow profile evolution is denoted by 'ODT line'. (b) Horizontal wind velocity components as function of height for turbulent and laminar flow. 100 instantaneous velocity profiles, uniformly sampled from four inertial periods of a transient ODT simulation for $Re = 500$, are plotted on top of each other to give an impression of the fluctuations (gusts).

2 Method

2.1 Flow configuration for the neutrally stratified ABL

Figure 1(a) shows a sketch of the idealized, neutrally stratified ABL configuration investigated. The set-up is identical to the isothermal calibration case described in [5] and consists of a pressure-driven bulk flow G, which is in geostrophic balance at height H far above the surface. The driving geostrophic pressure gradient points in spanwise (y) direction, but it is not directly resolved. Instead, the bulk velocity G is prescribed in streamwise (x) direction in order to kinematically parameterize the geostrophic forcing. The flow is described relative to the frame of reference that rotates around the vertical (z) coordinate with the local angular velocity $\Omega = f/2$, where f is the local Coriolis parameter. A smooth, flat surface is prescribed at $z = 0$ by homogeneous no-slip wall boundary conditions ($u = v = w = 0$). Conversely, zero-flux (homogeneous Neumann) boundary conditions are prescribed at $z = H$ in the free stream. This top boundary condition is of secondary importance as it resides well separated from the near-wall turbulence in the uniform bulk flow that acts as momentum reservoir.

The idealized ABL flow is fully is characterized by the Reynolds number, $Re = GD/\nu$, where ν is the kinematic viscosity of the fluid and $D = \sqrt{2\nu/f}$ is an estimator for the surface-layer thickness (laminar Ekman layer thickness, e.g. [18]) that serves as a reference length scale.

Figure 1(b) shows that the mean flow reaches a statistically steady state despite notable fluctuations. A statistically stationary state is obtained for laminar and turbulent conditions due to the Coriolis effect that has an influence on the vertical momentum transport. The mean state is characterized by a fixed boundary layer height, which is determined by the shear stress balance and is, hence, re-

lated to the Reynolds number Re. The domain height H needs to be large enough to accommodate the turbulent boundary layer thickness $\delta_\star = u_\star/f \gg D$, where $u_\star$ denotes the friction velocity, defined in section 3. The adaptive grid used in this study permissively resolves the viscous sublayer thickness $\delta_\nu = \nu/u_\star \ll D$. Further details on the numerical set-up are given in [5].

2.2 Overview of the stochastic model formulation and of its application to the ABL

Kerstein's one-dimensional turbulence (ODT) model [14] aims to resolve all relevant scales of a turbulent flow along a single physical coordinate. For the standalone modeling of atmospheric boundary layers [5, 15, 16], the single physical coordinate of the model (ODT line) is aligned with the vertical direction as sketched in figure 1(a). The ODT model equations are based on a dimensionally reduced form of the Navier–Stokes equations simplified by the boundary-layer approximation [19], adopted for the instantaneous variables. The vector-valued model equation governing the evolution of the instantaneous velocity profile of the neutrally stratified ABL is given by [5, 17]

$$\frac{\partial u_i}{\partial t} + \mathcal{E}_i = \nu \frac{\partial^2 u_i}{\partial z^2} - f\,\varepsilon_{i3k}\,(u_k - G\,\delta_{1k})\,, \tag{1}$$

where, in addition to the variables introduced above, t denotes the time, $(u_i) = (u, v, w)^{\mathrm{T}}$ the Cartesian components of the velocity vector with indices $i, j, k \in \{1, 2, 3\}$, δ_{ij} the Kronecker delta, ε_{ijk} the Levi–Civita tensor, and $\mathcal{E}_i$ the stochastic point process that models the effects of turbulent eddies. $\mathcal{E}_i$ addresses conservation properties so that the continuity equation is omitted. Further details can be found in [15], but in order to make the following results comprehensible, it is worth to elaborate on a few details.

$\mathcal{E}_i$ vanishes in between any two successive eddy events. The laminar response of the flow profiles during such time intervals is resolved on all scales along a one-dimensional physical coordinate and influenced by prescribed initial and boundary conditions. The continuous time integration is punctuated by eddy events implemented as a spatial mapping of flow profiles. Figure 2 shows a sketch of the so-called triplet map $M(z)$ that is used here. The physical mapping brings fluid elements from vertical location $M(z)$ to the mapped location z. The map is characterized by the size ℓ and the lower edge location z_{e}, which are both random variables in the stochastic sampling procedure [14]. In addition to the mapping rule that models turbulent advection, additional profile modifications are applied in order to model the effects of pressure–velocity couplings that are linked to an inter-component kinetic energy redistribution for incompressible flow [15]. The redistribution ratio among the velocity components is kept fixed to yield the fastest return to local isotropy.

Considering an instantaneous velocity profile, the sampling of a discrete eddy size ℓ and a vertical location z_{e} results in a momentary eddy rate given by the inverse of the corresponding eddy turnover time τ, that is, $\tau^{-1} = C\sqrt{2E/\ell^2}$,

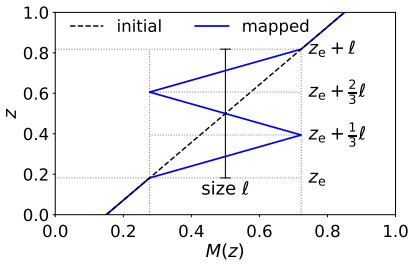

Fig. 2: Visualization of the triplet map $M(z)$ that implements a turbulent baker's map. The map is used to model the turbulent microstructure associated with a selected size-ℓ eddy event. A measure-preserving mapping rule is used to address physical conservation properties.

where $E = E_{\mathrm{kin}} - E_{\mathrm{pot}} - Z\,E_{\mathrm{vp}}$ represents the total energy available for a turbulent eddy under consideration, C is the eddy rate parameter, and Z the viscous suppression parameter. E has kinetic energy (E_{kin}) and potential energy (E_{pot}) contributions, as well as a viscous energy penalty (E_{vp}). For neutral stratification, E_{pot} vanishes identically. The individual contributions are obtained directly from the instantaneous flow profiles. Only eddies with $E > 0$ and net available energy in two of the three triplet map images (see figure 2) are deemed physical and subject to probabilistic acceptance. All other candidate eddy events are deemed unphysical and are, hence, rejected. The eddy rate expression and model calibration are not given here, but can be found, for example, in [5, 15, 16].

3 Results and discussion

3.1 Surface drag law

Figures 3(a) and 3(b) show the mean wind veer at the surface and the surface resistance, respectively, as functions of Re. ODT results are shown in comparison to available reference values from direct numerical simulation (DNS) [20, 21] and theory [22]. The wind veering angle α_0 and the friction velocity $u_\star$ are both defined at the surface and are obtained from the time-averaged horizontal velocity components, $U(z) = \overline{u(z,t)}$ and $V(z) = \overline{v(z,t)}$, as

$$\alpha_0 = \arctan\left(\left.\frac{\mathrm{d}V/\mathrm{d}z}{\mathrm{d}U/\mathrm{d}z}\right|_{z=0}\right), \qquad u_\star = \sqrt{\nu \left.\frac{\mathrm{d}\sqrt{U^2+V^2}}{\mathrm{d}z}\right|_{z=0}}. \tag{2}$$

The present model calibration aims to reproduce the wind turning effect but compromises on the friction velocity and, hence, the magnitude of the wall-shear stress. The wind turning effect, that is, the relative split between the two horizontal components of the wall-shear stress, is considered as one of the most crucial physical properties of ABL turbulence. Deviations in α_0 are, hence, deemed less acceptable than deviations in $u_\star$. The low-Re ($Re \leqslant 500$) calibration with $Z = 200$ and the high-Re ($Re > 500$) calibration with $Z = 1$, respectively, assure that ODT reproduces the reference wind veering angle at the surface with a low deviation in the friction velocity for all Re investigated. The approximate empirical asymptotic relation, $G/u_\star = 4 \ln Re - 8$, is met demonstrably better for $Z = 1$, although the agreement is not perfect.

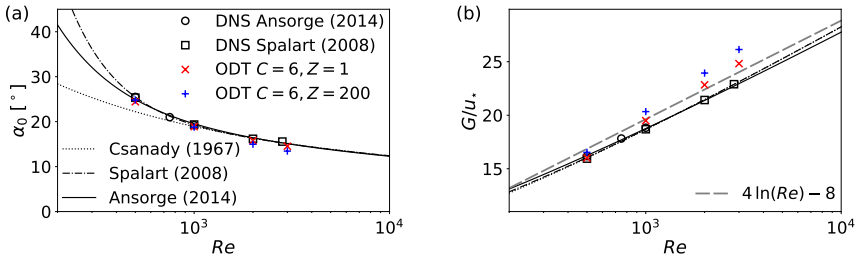

Fig. 3: (a) Mean wind veer at the surface and (b) inverse friction velocity as function of Re for turbulent flow using two different ODT model calibrations. Reference data is from [20–22].

3.2 Vertical profiles of the horizontal wind velocity components

Figure 4 shows wind velocity profiles for various Re that have been simulated with ODT. Time-averaged profiles, $U(z), V(z)$, and instantaneous profiles, $u(z, t = t_0), v(z, t = t_0)$, are shown. At low Re, turbulence is weak and fluctuations are associated with very large deviations from the mean flow. As the Re increases, more small-scale features and seemingly less severe excursions from the mean are discerned. The schematic wind turbine that is given at the bottom right in each panel visualizes the size relation between a tall wind turbine and the height of the ABL for a size-to-height ratio of 10%. It is apparent that a wind turbine can exhibit significant fluctuations, nonuniform wind veer, and nonzero wind shear across its rotor.

3.3 Temporal evolution of the instantaneous wind velocity profile

Figure 5 shows a synopsis of the ODT flow profile evolution. Figures 5(a) and 5(b) highlight the emerging features of the piecewise continuous flow evolution showing contours of the streamwise velocity and the model-resolved streamwise

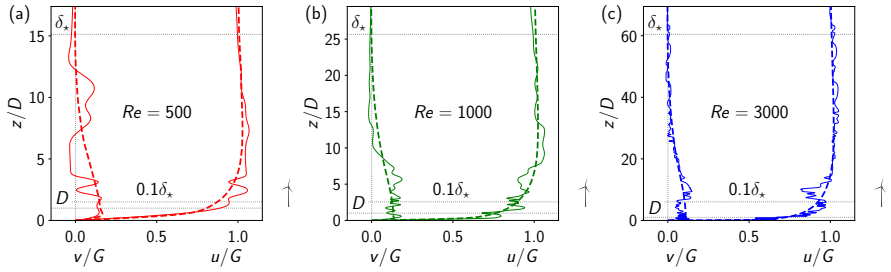

Fig. 4: Instantaneous and time-averaged profiles of the horizontal wind components for various Re scaled to the same ABL height $\delta_\star$. Sketched wind turbines have their hub height at $0.1\,\delta_\star$.

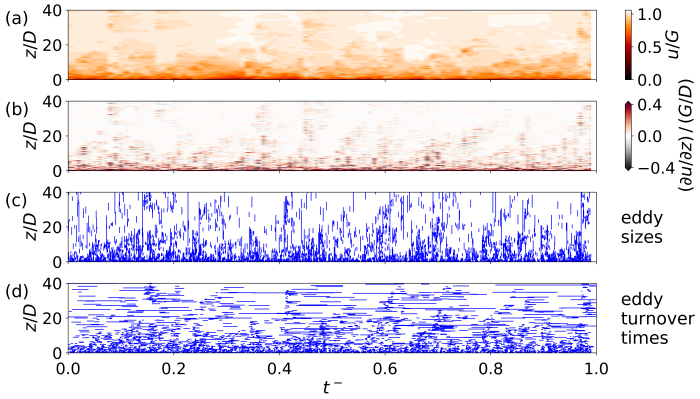

Fig. 5: ODT flow evolution of the neutrally stratified ABL with $Re = 3000$ across an inertial period, $0 \leqslant t^- = t/(2\pi f^{-1}) \leqslant 1$, in the statistically stationary state. (a) Streamwise velocity, (b) streamwise velocity shear, (c) sequence of the stochastically sampled eddy events visualizing the vertical intervals $[z_\mathrm{e}, z_\mathrm{e} + \ell]$, and (d) corresponding sequence of the eddy turnover time intervals $[t_\mathrm{e}, t_\mathrm{e} + \tau]$ located at the eddy occurrence time t_e and the eddy mid point $z_\mathrm{m} = z_\mathrm{e} + \frac{\ell}{2}$.

velocity shear, respectively. The flow features are reminiscent of turbulent bursts, microfronts, and uniform momentum zones (e.g. [3, 4]), although no feature attribution is suggested here. Figures 5(c) and 5(d) highlight the discrete evolution of the turbulent flow by the sequence of the stochastically sampled eddy events. This sequence represents labeled data that encodes physical information on the evolving flow state. With this data it is possible to retrieve the participating spatial and temporal scales that are not directly accessible from the instantaneous flow profile.

3.4 Temporal intermittency

Figure 6 shows simulated time series of the fluctuating streamwise velocity $u(z = D, t)$ at a selected level height for various Re. The level height $z = D$ has been selected in order to sample velocity fluctuations in the inner, near-wall region of the logarithmic layer of the ABL, which is elaborated in [5]. The most important feature is to be seen in sudden velocity changes (gusts) that are exhibited for all Re investigated. These features are traces of intermittency, which is a salient property of turbulence. A piecewise averaging is performed in order to demonstrate that the wind gusts may lead to unsteady flow behavior, even on time scales which are as large as a fifth of an inertial period, and at altitudes in the logarithmic layer.

Figures 7(a) and 7(b) show probability density functions (p.d.f.) of the streamwise and spanwise velocity fluctuations corresponding to the time series shown above. The streamwise (u') and spanwise (v') velocity fluctuations at altitude $z = D$ are normalized by the standard deviation (root mean square, r.m.s.) of

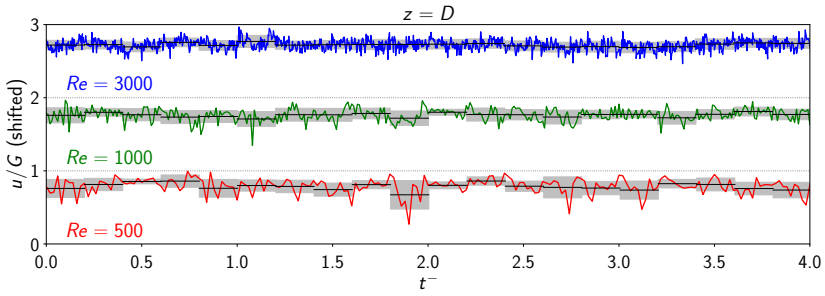

Fig. 6: Time series of the streamwise velocity at level height $z = D$ simulated with ODT covering four inertial periods, $0 \leqslant t^- = t/(2\pi f^{-1}) \leqslant 4$. Piecewise averaging is performed over time intervals of size $\Delta t^- = 0.2$. Corresponding means and standard deviations are indicated.

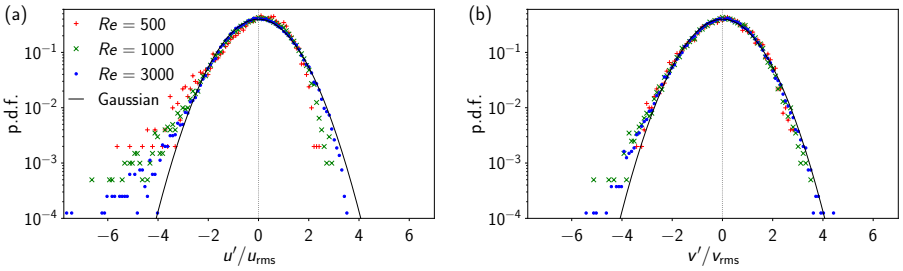

Fig. 7: Estimated probability density function (p.d.f.) corresponding to the time series in figure 6. ODT data stems from extended single realizations covering tens of intertial periods.

the long-time average, $u_{\mathrm{rms}} = \sqrt{\overline{u^2} - U^2}$ and $v_{\mathrm{rms}} = \sqrt{\overline{v^2} - V^2}$, respectively. Notable intermittent, non-Gaussian behavior is discerned for rare events associated with fluctuations exceeding three standard deviations. These intermittency effects, as predicted by the model, are strongest for negative u' and weakest for positive v'.

4 Concluding remarks

A map-based stochastic forward modeling strategy has been presented and applied to the neutrally stratified ABL. Various turbulence intensities have been investigated by variation of the relative strength of the driving mean pressure gradient, parametrized by the prescribed geostrophic wind velocity. The presented approach specifically addresses some predictive capabilities of the one-dimensional turbulence (ODT) model that are relevant for volatility assessment and short-term forcasting of available wind power under evolving wind conditions. Forthcoming research is devoted to the development of a numerical tool

that can be used to address turbulence in two distinct use cases. The first use case is the post-processing of operational NWP data to minute-scale forecasts at a given site, which may be accomplished by extending the model application shown in [23]. The second use cases is the synthetic generation of inflow velocity profiles for the pre-design of wind turbines, improving the representation challenging atmospheric conditions.

Acknowledgment

The authors thank Joseph Gerardi for editing the English language.

This research is supported by the German Federal Government, the Federal Ministry of Education and Research, and the State of Brandenburg within the framework of the joint project EIZ: Energy Innovation Center (project numbers 85056897 and 03SF0693A) with funds from the Structural Development Act (Strukturstärkungsgesetz) for coal-mining regions.

References

1. Holtslag, A.A.M., Svensson, G., Baas, P., Basu, S., Beare, B., Beljaars, A.C.M., Bosveld, F.C., Cuxart, J., Lindvall, J., Steeneveld, G.J., Tjernström, M., Van De Wiel, B.J.H.: Stable atmospheric boundary layers and diurnal cycles: Challenges for weather and climate models. Bull. Am. Meteorol. Soc. **94**(11), 1691–1706 (2013). DOI 10.1175/BAMS-D-11-00187.1
2. Haupt, S.E., Kosović, B., Berg, L.K., Kaul, C.M., Churchfield, M., Mirocha, J., Allaerts, D., Brummet, T., Davis, S., DeCastro, A., Dettling, S., Draxl, C., Gagne, D.J., Hawbecker, P., Jha, P., Juliano, T., Lassman, W., Quon, E., Rai, R.K., Robinson, M., Shaw, W., Thedin, R.: Lessons learned in coupling atmospheric models across scales for onshore and offshore wind energy. Wind Energ. Sci. **8**(8), 1251–1275 (2023). DOI 10.5194/wes-8-1251-2023
3. de Silva, C.M., Hutchins, N., Marusic, I.: Uniform momentum zones in turbulent boundary layers. J. Fluid Mech. **786**, 309–331 (2016). DOI 10.1017/jfm.2015.672
4. Ehsani, R., Heisel, M., Li, J., Voller, V., Hong, J., Guala, M.: Stochastic modelling of the instantaneous velocity profile in rough-wall turbulent boundary layers. J. Fluid Mech. **979**, A12 (2024). DOI 10.1017/jfm.2023.999
5. Klein, M., Schmidt, H.: Exploring stratification effects in stable Ekman boundary layers using a stochastic one-dimensional turbulence model. Adv. Sci. Res. **19**, 117–136 (2022). DOI 10.5194/asr-19-117-2022
6. Neuhaus, L., Wächter, M., Peinke, J.: The fractal turbulent–non-turbulent interface in the atmosphere. Wind Energ. Sci. **9**(2), 439–452 (2024). DOI 10.5194/wes-9-439-2024
7. Porté-Agel, F., Bastankhah, M., Shamsoddin, S.: Wind-turbine and wind-farm flows: A review. Bound.-Lay. Meteorol. **174**, 1–59 (2020). DOI 10.1007/s10546-019-00473-0
8. Reinert, D., Prill, F., Frank, H., Denhard, M., Baldauf, M., Schraff, C., Gebhardt, C., Marsigli, C., Zängl, G.: DWD Database Reference for the Global and Regional ICON and ICON-EPS Forecasting System, Version 2.2.2. Deutscher Wetterdienst, Offenbach am Main, Germany (2021). URL https://www.dwd.de/DWD/forschung/nwv/fepub/icon_database_main.pdf

9. Muschinski, T., Lang, M.N., Mayr, G.J., Messner, J.W., Zeileis, A., Simon, T.: Predicting power ramps from joint distributions of future wind speeds. Wind Energ. Sci. **7**(6), 2393–2405 (2022). DOI 10.5194/wes-7-2393-2022
10. Kelley, N.D., Jonkman, B.J.: Overview of the TurbSim stochastic inflow turbulence simulator. Tech. Rep. NREL/TP-500-41137, National Renewable Energy Laboratory (2007)
11. Boyko, V., Vercauteren, N.: A stochastic stability equation for unsteady turbulence in the stable boundary layer. Q. J. R. Meteorol. Soc. **149**(755), 2125–2145 (2023). DOI 10.1002/qj.4498
12. Sommerfeld, M., Dörenkämper, M., De Schutter, J., Crawford, C.: Impact of wind profiles on ground-generation airborne wind energy system performance. Wind Energ. Sci. **8**(7), 1153–1178 (2023). DOI 10.5194/wes-8-1153-2023
13. Yassin, K., Helms, A., Moreno, D., Kassem, H., Höning, L., Lukassen, L.J.: Applying a random time mapping to mann-modeled turbulence for the generation of intermittent wind fields. Wind Energ. Sci. **8**(7), 1133–1152 (2023). DOI 10.5194/wes-8-1133-2023
14. Kerstein, A.R.: One-dimensional turbulence: Model formulation and application to homogeneous turbulence, shear flows, and buoyant stratified flows. J. Fluid Mech. **392**, 277–334 (1999). DOI 10.1017/S0022112099005376
15. Kerstein, A.R., Wunsch, S.: Simulation of a stably stratified atmospheric boundary layer using one-dimensional turbulence. Bound.-Lay. Meteorol. **118**, 325–356 (2006). DOI 10.1007/s10546-005-9004-x
16. Freire, L.S., Chamecki, M.: A one-dimensional stochastic model of turbulence within and above plant canopies. Agric. For. Meteorol. **250-251**, 9–23 (2018). DOI 10.1016/j.agrformet.2017.12.211
17. Klein, M., Schmidt, H.: Capturing features of turbulent Ekman–Stokes boundary layers with a stochastic modeling approach. Adv. Sci. Res. **20**, 55–64 (2023). DOI 10.5194/asr-20-55-2023
18. Pedlosky, J.: Geophysical Fluid Dynamics. Springer, New York (1979). DOI 10.1007/978-1-4684-0071-7
19. Schlichting, H., Gersten, K.: Boundary-Layer Theory. Springer, Berlin (2000). DOI 10.1007/978-3-642-85829-1
20. Ansorge, C., Mellado, J.P.: Global intermittency and collapsing turbulence in the stratified atmospheric boundary layer. Bound.-Lay. Meteorol. **153**, 89–116 (2014). DOI 10.1007/s10546-014-9941-3
21. Spalart, P.R., Coleman, G.N., Johnstone, R.: Direct numerical simulation of the ekman layer: A step in reynolds number, and cautious support for a log law with a shifted origin. Phys. Fluids **20**(10), 101,507 (2008). DOI 10.1063/1.3005858
22. Csanady, G.T.: On the "resistance law" of a turbulent Ekman layer. J. Atmos. Sci. **24**(5), 467–471 (1967)
23. Glawe, C., Klein, M., Schmidt, H.: Stochastic deconvolution of wall statistics in Reynolds-averaged Navier–Stokes simulations based on one-dimensional turbulence. Proc. Appl. Math. Mech. **23**(3), e202300055 (2023). DOI https://doi.org/10.1002/pamm.202300055